

# Clustering Image Noise Patterns By Embedding And Visualization For Unknown Source Camera Detection

S.SARAVANA<sup>1</sup>, Prof T.ANURADHA<sup>2</sup>

<sup>1,2</sup>Department of Computer Science Dravidan University Kuppam – 517426 A.P INDIA

Email: <sup>1</sup>ssaravana\_ssi@yahoo.co.in, <sup>2</sup>rajamaata@yahoo.co.in

**ABSTRACT:** *We consider the problem of clustering a large set of images based on similarities of their noise patterns. Such clustering is necessary in forensic cases in which detection of common source of images is required, when the cameras are not physically available. We propose a novel method for clustering combining low dimensional embedding, visualization, and classical clustering of the dataset based on the similarity scores. We evaluate our method on the Dresden images database showing that the methodology is highly effective.*

**Keywords:** *Clustering; digital camera identification; common image source detection; Photo-response non-uniformity; Digital forensics*

## 1. INTRODUCTION

Common source identification of digital photographs can play an important role in digital investigations. The identification problem exists because the meta-data accompanying the image can be easily altered by the creators to remove traces of its origin. Nevertheless, it has been found that small deficiencies in the imaging sensor of a camera leads to detectable noise in the image, so-called Photo-Response Non-Uniformity (PRNU) patterns (Lukas et al., 2006), which provides a signature that can be used to identify the source of an image in a robust

manner.

When a suspect camera is present, its PRNU fingerprint can be estimated from the set of images taken by it. Then, the fingerprint can be used on images to determine whether they originated from the corresponding camera.

Prevailing with regards to portraying data about the birthplace of an advanced picture is a basic issue of sight and sound legal sciences. It is easy to comprehend that in various application situations data at expulsion are exceptionally restricted; this is the situation while, given an arrangement of  $N$  pictures, to establish on the off chance that they have a place with  $M$  different cameras where  $M$  is less or, at most, equivalent to  $N$ , without containing some information about the source cameras. In this postulation, a novel technique which goes for aimlessly bunching a given arrangement of  $N$  computerized pictures is presented. Such a technique is relying upon a prior one [71] and improves it both as far as blunder likelihood and of computational

viability. The strategy is able, in an unsupervised and quick technique, to amass photographs without some underlying data about their enrollment.

Sensor design commotion is determined by each picture as reference and the progressive arrangement is executed by methods for a various leveled bunching process. Exploratory outcomes have been done to affirm hypothetical desires and to witness the advancements regarding the other strategy. Tests have additionally been done in different agent conditions (e.g. Hitler kilter designation of the pictures inside each bunch), getting acceptable outcomes.

## 2. UNDERPINNING TECHNOLOGIES, METHODS AND TOOLS

Since Photo Response Non-Uniformity (PRNU) is a piece of the high-recurrence segments of the picture's flag, it can be utilized the model in condition (5.1), so as to concentrate the commotion  $n$  from a picture

$$n = I - F(I) \quad (5.1)$$

where  $F$ , is a wavelet-based denoising filter that filters out the sensor pattern noise of the image.

Then again, not all the high-recurrence picture segments are in charge of the sensor design clamor: actually, scene points of interest likewise add to these segments and their augmentation is typically more prominent than that of PRNU. Consequently the clamor  $n$  ought to be cleaned from scene points of interest to advance the framework execution. This wok turns out to be immensely basic to get just a little picture hinder into depiction: on the one section a little piece helps by diminishing the computational time, on the other part it can lose a great deal of data. In the work displayed in it has been enhanced a function that means to sift through scene points of interest, contingent upon the accompanying thought: scene subtle elements add to the exceptionally solid flag parts, in this manner the more grounded a flag segment (in  $n$ ), the more it is lessened. As per this thought, another sort of enhancer has been made strides. The clamor improving capacity gives greater weighting elements to the feeble parts of  $n$  in the DWT area, and vice versa, and it is characterized by the formulae in condition (5.2):

$$n_e = \begin{cases} 0 & n(i,j) < -\alpha \\ -\cos(n(i,j)\pi/2\alpha) & -\alpha \leq n(i,j) \leq 0 \\ \cos(n(i,j)\pi/2\alpha) & 0 < n(i,j) \leq \alpha \\ 0 & n(i,j) > \alpha \end{cases} \quad (5.2)$$

where  $\alpha$  is a parameter that describes the cut value between the PRNU components and the scene details (figure 5.1).

The accumulation of the parameter  $\alpha$  has been accomplished by methods for an arrangement of source camera acknowledgment tests. On an arrangement of 1200 photographs, taken from 6 different cameras (i.e. 200 for every), little pieces of  $128 \times 128$  pixels edited from the first photographs were used to assess the execution while contrasting the parameter  $\alpha$  to acquire the best one. Six reference NUs were created by assessing the normal of the clamors extricated from 50 photographs taken by each advanced camera, without utilizing any expanding capacity. Thusly, these

fingerprints were used to classify a test-set (made by 600 photographs, 100 from each camera, fluctuates from those utilized for the reference PRNUs) by essentially assessing the relationship between's the present commotion (extracted with the use of the expanding capacity) and everybody of the six reference PRNUs and regarding the picture as taken by the camera identified with the most extreme of the connection values. The best order execution was accomplished with  $\alpha \in [0.05, 0.0575]$  with 504/600 right groupings, corresponding to a 84% rate (figure 5.2) however the pattern is steady beginning from  $\alpha = 0.04$ .

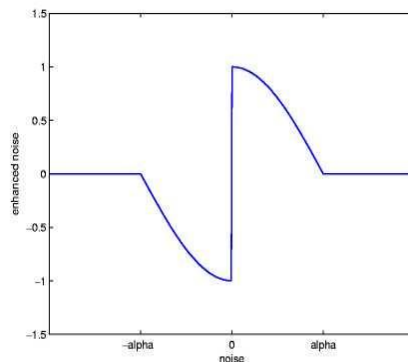


Figure 5.2 Enhancement function

The performance of this test without the use of an enhancing function is only 215/600 (35.8%): that's what it is expected from the previous considerations.

### 2.1 Interactive visualization of the Dresden image database

The point of this procedure is to quickly classify a nonexclusive gathering of photographs taken by different cameras, in an altogether unsupervised mode. Beginning from the strategy has been endeavored to create execution as far as calculation speed and exactness assessment. To do this a few bunching calculation relying upon progressive grouping has been introduced .Hierarchical bunching yields a chain of importance of bunches which might be and B is assessed by the Equation (5.3):

$$H(A, B) = (1/||A|| ||B||) \sum_{n_i \in A, n_j \in B} \text{corr}(n_i, n_j) \quad (5.3)$$

where  $\text{corr}(n_i, n_j)$  is the normalized correlation (equation 5.4)

$$\text{Corr}(n_i, n_j) = (n_i \cdot \bar{n}_j) / (||n_i - \bar{n}_i|| ||n_j - \bar{n}_j||) \quad (5.4)$$

While  $||A||$  and  $||B||$  are the cardinalities of the considered clusters. It is profitable to state that H can be a symmetric grid with ones on the significant slanting, whose components  $H(k,l)$  relate to the likeness between bunches k and l. The underlying lattice H is a  $N \times N$  network that has the simple connections among the commotions  $n_1, \dots, n_N$ , in this way it is refreshed by disposing of lines/segments related to the groups that have been converged by including lines/segments related to the new combined bunch and by reconsidering the similarity values between the new group and each staying ones. Various leveled bunching does not require a pre-determined number of groups. On the other hand, in this application, a segment of disjoint groups similarly as in level bunching: for this situation, the chain of importance requires to be cut at a few focuses. Different criteria is used to set up the cutting point: the paradigm relying upon the outline coefficient is used. The use of outline coefficient joins both the measures of union (inside bunches) and partition (among

groups). For each clamor  $n_i$ , the coefficient  $s_i$  is quite recently figured as in condition (5.5):

$$s_i = b_i - a_i \quad (5.5) \quad 1) \quad a_i$$

**(cohesion):** The average correlation of  $n_i$  to all other noises in the same cluster.

**2)  $b_i$  (separation):** The average correlation of  $n_i$  to all other noises in each of the other clusters, taking the average value with respect to all clusters.

For instance, an exceptionally negative estimation of  $s_i$  implies that the segment esteem  $b_i$  is profoundly negative and the union ( $a_i$ ) is extremely positive: this means what has been combined is really associated. Subsequently the procedure goes for the littlest likely estimation of the outline coefficient to accomplish a decent bunching. To relate this figuring at each circle of the calculation and at each commotion in the information are looking at: all the more precisely, at the cycle  $q$  it is expected a worldwide measure of the outline coefficient  $SC_q$  (condition 5.6) by averaging the coefficients related to each clamor that have a place with a distinct group and bringing the normal incentive as for each present  $K$ -bunches.

$$SC_q = 1/N \sum_{i=1}^N s_i \quad (5.6)$$

In this way it is found the base coefficient over the  $N - 1$  got and the comparing file  $q^*$  is chosen as the cycle that must be taken as the last to be actualized. As per this, grouping ought to be done again with the found stop condition; on the other hand it has been used an adroitness to spare execution time that contains in sparing at each circle the present parcel  $P_q$ , and a while later picking the ideal bunching by simply utilizing the segment  $P_{q^*}$ . Here is the pseudo-code of the calculation embraced:

1. Initialization:  $K \leq N$ , calculate similarity matrix  $H \in R^{N \times N}$
2. Loop over  $q \leq 1$  to  $N-1$ 
  - (a) Search for the pair of clusters  $\{U, V\}$  that match the greatest similarity
  - (b) Delete from  $H$  the rows and the columns referred to clusters  $\{U, V\}$
  - (c) Update  $H$  by calculating the new similarity values between the new cluster  $Z \leq \{U, V\}$  and the remaining clusters
  - (d)  $K \leq K - 1$
  - (e) Calculate the silhouette coefficient  $SC_q$
  - (f) Save the current partition  $P_q$
3. Calculate the minimum value of the silhouette coefficients:  
 $q^* \leq \min_q(SC_q)$
4. Get the optimal partition by selecting the one relative to the iteration  $q^*$ , that is the partition  $P_{q^*}$ .

Toward the finish of the grouping technique, the quantity of bunches  $M$  is acquired, that should be precisely the genuine number of gadgets which created the given  $N$  pictures of the preparation set. For each one of the got  $M$  clusters, a reference commotion is evaluated (as the group centroid) essentially by averaging each clamors relating to that bunch. The centroids of the bunches given by the said handled are then used as the prepared classifier to amass the pictures relating to the test set. The arrangement is simple: it contains on contrasting the likeness of the present picture to everything about centroids, and next order the picture to the bunch whose centroid is what gives the best similitude.

Table :1 Training phase (or clustering phase) TPR (True Positive Rate) for the PRNU method (with and without enhancer)

TPR vs Size	128 x 128	128 x 256	256 x 256	256 x 512	512 x 512	1024 x 1024	1536 x 2048
no enhancer	24.1%	27.3%	24.3%	26.3%	26.5%	38.9%	98.5%
with enhancer	51.7%	79.3%	87.3%	96.3%	98.0%	98.7%	99.8%
PRNU Method	52.3%	80.0%	87.7%	96.1%	97.3%	98.8%	NA

Table :2 Training phase: comparison between with enhancer method and PRNU method in terms of execution time (in seconds)

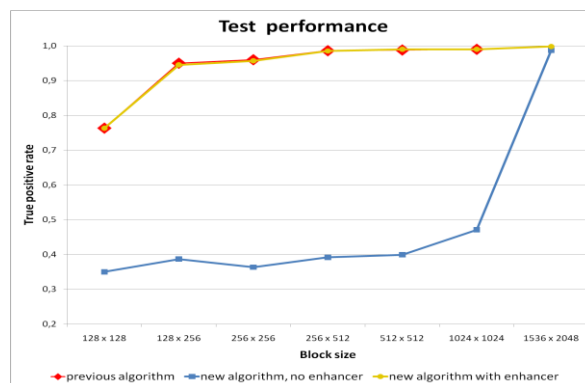
TPR vs Size	128 x 128	128 x 256	256 x 256	256 x 512	512 x 512	1024 x 1024	1536 x 2048
with enhancer	876	1053	1108	1146	1452	3166	5104
PRNU Method	16183	16200	16284	16437	12215	13896	Not tested

## 2.2 The proposed methodology for clustering

To affirm the exhibitions of the introduced daze bunching process the strategy has been tried on a dataset populated by 1200 photographs at different resolutions (from 3MP to 12MP) taken by six cameras in different day and age (200 photographs for each camera), here are the cameras: Canon EOS400D (10MP), Canon Digital Ixus i zoom (5MP), Canon Digital Ixus II (3MP), Panasonic DMC-FX12 (7MP), Sony DMC-LZ5 (6MP), FujiFilm FinePix J20 (12MP). Different examinations have been completed in various agent conditions:



(a)



(b)

Figure:5.2 Training phase (a) Clustering (b) Test performances

1. Image blocks of different sizes, from  $128 \times 128$  to  $1536 \times 2048$  pixels;
2. Using or not a PRNU enhancer;
3. Training set and test set with a symmetric or an asymmetric distribution of the images within each cluster.

In the primary analysis, it has been utilized a uniform appropriation of the pictures (same number of pictures for each cameras) both for the preparation set and for the test set. The measurement of the preparation set was of 300 pictures (50 pictures for every camera), while the test set measurement was of 600 (100 pictures for each camera). Moreover, not to get deceiving assessment of exhibitions, covering between the two informational collection has been stayed away from. Along these lines the TPR (True Positive Rate) and the preparing time for this calculation (with and without enhancer) are contrasted and the technique [71]. The TPR identified with the preparation stage (or grouping stage) gotten by varying the picture piece measurement is accounted for in table 5.1. The TPR accomplished for the utilized calculation (with enhancer) (second column in table 5.1) and for the calculation [71] (third line in table 5.1) are practically identical for all picture square sizes yet this calculation is conceivable to achieve higher picture piece determination and thusly better TPR (table 5.1).

This is because of the way that this technique performs better in term of time execution as revealed in table 5.2 (around 14 minutes against over 4 hours for the littler piece measure in the main segment). From that point onward, a testing eliminate has been conveyed to assess the exhibitions of this technique and the outcomes are appeared in figure 5.2(b). The outcomes are practically identical in term of TPR to the outcomes acquired amid the preparation stage (or grouping stage) as revealed in figure 5.2(a). It is conceivable to bring up that utilizing enhancer turns out to be less essential when picture piece of higher determination are considered that is when moving toward the genuine picture determination. In the second examination, the strength of this calculation regarding a non uniform informational index has been tried and a correlation with the calculation [71] has been made.

Five different gatherings have been produced for the preparation set as the test set is the same as some time recently. For each gathering the difference for the quantity of pictures having a place with each camera is improved, as table 5.3 uniform datasets (bunches D, E). Moreover, with this calculation is conceivable to assess the execution for the picture piece determination  $1024 \times 1024$  achieving a TPR of 86.5% notwithstanding for the gathering E. This sort of analysis is not really achievable for the calculation [71] because of its high computational time as appeared in table 5.3. In table 5.4 the TPR for preparing and test stage

identified with this technique is accounted for and table 5.5 the outcomes gotten for the strategy [71] are appeared.

Table5.3 Non uniform data set distribution

Group	Cam 1	Cam 2	Cam 3	Cam 4	Cam 5	Cam 6
A	55	45	55	45	55	45
B	60	40	60	40	60	40
C	70	30	70	30	70	30
D	80	20	80	20	80	20

Table 5.4 TPR in the PRNU method for 1024x1024, 512x512, 256x256 (a)training (b) testing

TPR vs Size	A	B	C	D	E
1024x1024	95.2%	92.0%	84.8%	76.8%	68.4%
512x512	89.3%	87.6%	80.0%	71.0%	56.0%
256x256	82.1%	76.7%	75.3%	66.5%	53.0%

(a)

TPR vs Size	A	B	C	D	E
1024x1024	97.8%	96.3%	94.7%	91.2%	86.5%
512x512	93.3%	91.0%	87.6%	84.9%	82.6%
256x256	89.8%	84.4%	82.5%	73.1%	61.1%

(b)

Table 5.5 TPR in the PRNU method for 512x512, 256x256 (a) training (b) testing

TPR vs Size	A	B	C	D	E
512x512	89.7%	87.3%	79.0%	69.3%	49.7%
256x256	81.9%	77.4%	74.9%	66.5%	46.3%

(a)

TPR vs Size	A	B	C	D	E
512x512	94.0%	91.6%	86.6%	79.8%	56.2%
256x256	89.8%	83.9%	81.6%	72.1%	50.9%

(b)

The two calculations have comparable exhibitions identified with the gathering A, B and C, while the new calculation indicates better exhibitions especially for non uniform datasets (bunches D, E). Moreover, with this calculation is likely to evaluate the execution for the picture square determination 1024×1024 accomplishing a TPR of 86.5% notwithstanding for the gathering E. This sort of test is not really practical for the calculation [71] because of its high computational time as appeared in table 5.2.

### 3. PERFORMANCE COMPARISON BETWEEN CAMERA AND SCANNED IMAGES

Separating the sort of sensor which has procured an advanced picture could be essential in various situations where computerized criminological strategies are called to give answers. In this section, a sensor design clamor innovation is to set up if an advanced photograph has been taken by a camera or has been filtered by a scanner. Such a technique utilize the distinct geometrical components of the sensor design clamor displayed by the sensor in both cases and by depending on a recurrence investigation can assume if a periodicity is available and as needs be which is the computerized content beginning. Exploratory outcomes are exhibited to keep up the hypothetical structure.

#### 3.1 Sensor Pattern Noise Characterization

PRNU (Photo Response Non-Uniformity) clamor is moderately outstanding similar to a proficient instrument for sensor acknowledgment since it is deterministically created over each computerized picture it gets. Such a commotion is thusly an inborn normal for that positive sensor. This clamor extraction is much of the time accomplished by denoising channels [50] and data it used to evaluate something on the sensor qualities. In the event that attention is on the accomplishment procedure, it is easy to understand that while a photograph is taken by an advanced camera, in a general sense a PRNU with a bi-dimensional structure is superimposed to it; on the restricting, while a computerized picture is delivered by methods for a filtering operation the sensor exhibit which slides over the to-be-gained resource situated on the scanner plate leaves its mono-dimensional unique mark push by line amid examining. Thusly in the last case, it is unsurprising that an unequivocal periodicity of the 1-D clamor flag is prove along the scanning course. This execution ought to be absent in the camera case and this uniqueness can be explored to recognize pictures originating from the two different sorts of gadget. Being  $R(i,j)$  with  $1 \leq i \leq N$  and  $1 \leq j \leq M$ , by the filtered picture of size  $N \times M$ , the clamor removed and accepting  $i$  (push) as checking bearing, it can, in any event preferably, be likely that every one of the lines are equal.

$$R(i,j) = R(k,j) \quad \forall 1 \leq j \leq M, 1 \leq i, k \leq N \quad (5.7)$$

So if a 1-D signal,  $S$  of  $N \times M$  samples, is constructed by concatenating all the rows, it happens that  $S$  is a periodical signal of period  $M$ .

$$S = [R(1,1), \dots, R(1,M), \dots, R(N,1), \dots, R(N,M)] \quad (5.8)$$

It is likewise significant to call attention to that if the 1-D flag is mounted close to sections bearing (i.e. this would be correct expecting that  $j$  is the examining heading),  $S$  is not periodical any more, but rather it is constituted by different constant steps everything about  $M$ . A periodical flag, for example,  $S$ , spoke to condition 5.8, contains various redundancies equivalent to  $N$  thus can have basically a recurrence range made by equispaced spikes. Such spikes can be dispersed of  $(N \times M)/M = N$  and will be one-sided by the range of the basic multiplication of the flag. In this way, a large portion of the vitality of such a flag is situated in these spikes. Detectably, this is the thing that ought to happen, by and by the 1-D flag can be adulterated and its periodical structure altered. Thusly the ghostly spikes can be diminished and their degree incompletely spread over alternate frequencies. On the off chance that it is as

yet likely to individuate such pinnacles, it can be anything but difficult to separate between a filtered picture and a computerized photograph.

### 3.2 The PRNU Methodology

As per the thought exhibited in Section 5.1, a detail portrayal of the PRNU strategy is expected to accomplish that plan. The to-be-checked picture  $I$  (estimate  $N \times M$ ) is denoise sifted [50] getting  $I_d$  which is subtracted to the essential picture to extricate the sensor design commotion  $R$  (Equation 5.9)  $R = I - I_d$

To enhance the conceivable nearness of the deterministic commitment because of the 1-D PRNU design clamor,  $R$  is isolated into non-covering stripes (both vertically and on a level plane, in light of the fact that both likely examining bearings must be considered) and in this manner each different lines (sections) having a place with a stripe are found the middle value of as per Equation 5.10 where  $L$  is the thickness of the stripe.

$$R_r(r) = 1/L \sum_{i=r}^{i+(r-1)L} R[i+(r-1)L] \quad 1 \leq r \leq N/L \quad (5.10)$$

After that two new clamor pictures, named standardized identifications, separately  $R_r$  (estimate  $N/L \times M$ ) and  $R_c$  (measure  $N \times M/L$ ), have been gotten;  $R_r$  and  $R_c$  have a similar number of tests. In the event that a picture has been checked in the line heading, for example, it is normal that  $R_r$  will be created by equivalent (in a perfect world) lines, on the opposite side such a portrayal can not be normal in the section course for  $R_c$  and, most importantly, for a picture originating from a computerized camera (both bearings): this condition is exhibited in Figure 5.1. Scanner tags are then

used to make the mono-dimensional flag by connecting separately lines of  $R_r$  and sections of  $R_c$  and after that periodicity is checked. Once in a while to lessen arbitrariness a low pass sifting operation (generally a middle channel) is connected to scanner tags, along the lines and the segments independently, before developing 1-D signals.

For clearness,  $S_r$  and  $S_c$  are named as the two mono-dimensional flag, acquired as already depicted, from  $R_r$  and  $R_c$  individually. DFT (Discrete Fourier Transform) is connected to both these signs and the magnitude of the coefficients is considered. After that a determination is completed Figure 5.1: Bar codes of size  $N/L \times M$  (checking heading = push): camera picture (beat), examined picture (focus) and perfect standardized tag for a filtered picture (base) on the premise of the accompanying standard: estimations of adequacy over a limit  $2 \sim i$  and in the meantime situated in the normal positions inside the range are taken.

$$T1 = a * \max(\max(\text{abs}(\text{DFT}(S_r))), \max(\text{abs}(\text{DFT}(S_c)))) \quad (5.11)$$

At last every one of the qualities fulfilling the past gathering measure are included, unconnectedly for line and section cases, respecting two vitality variables,  $F_r$  and  $F_c$  individually and their proportion  $\text{RATIO} = F_r/F_c$  is processed. In the event that the computerized picture has been examined in the line heading, a high  $\text{RATIO}$  esteem is unsurprising (if the checking bearing has been along segments  $\text{RATIO}$  will be little), generally if the picture has been taken by an advanced camera the two vitality components ought to be equivalent and an estimation of  $\text{RATIO}$  around one is anticipated. Doing subsequently it is likely not just separating between pictures originating from a scanner or from a camera in any case, in the scanner case, portraying the filtering heading. To advance vigor, this technique is utilized to each three picture channels (R, G, B) and three vitality commitments are created in each element  $F_r$  and  $F_c$ .

### 3.3 Analysis Of Thresholds Through Roc curves

The limit T1, that is utilized to assess vitality of DFT of signs Sr and Sc, relies on  $\alpha$  parameter, other than there is another edge T2, for the RATIO esteem, that makes conceivable to recognize pictures taken from scanners or computerized cameras. Legitimate decision of these two parameters is a key issue to sufficiently control separation. To discover ideal incentive for T1 and T2, is conceivable to utilize ROC (Receive Operating Characteristic or Relative Operating Characteristic) Curve. To acquaint ROC Curve is fundamental with characterize two new parameters:

1. Se (Sensitivity): the division of pictures taken from a scanner effectively distinguished all things considered.
2. Sp (Specificity): the division of pictures taken from a computerized camera that are effectively distinguished in that capacity.

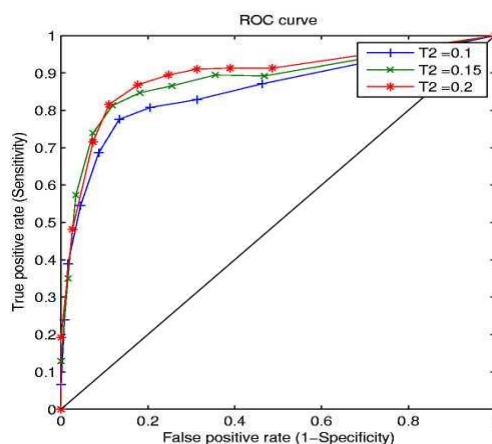


Figure 5.3 Roc Curves

Finding ideal edges is not restricted to the measurable minimization of wrong arrangement, however it is additionally related to the FRR (False Rejection Rate) minimization for scanner pictures or advanced camera pictures. ROC Curve grants to look at more estimations of the edges to build up which acquires the best outcomes. The ROC Curves examination is performed through the capacity that ties the likelihood of True Positive to perceive checked pictures (Se) and the likelihood to acquire a False Positive ( $1 - Sp$ ). The connection between these parameters can be spoken to by plotting Se on the y-hub and ( $1 - Sp$ ) on the x-pivot (figure 5.2). A solitary disarray framework (table 5.3) along these lines delivers a solitary point in ROC space. A ROC bend is shaped from a grouping of such focuses, including (0,0) and (1,1).

Table 5.6 Confusion matrix

	Camera	Scanner
Camera	$S_c$	$1-S_c$
Scanner	$1-S_s$	$S_s$

To decide the best estimation of  $\alpha$  for T1 is important to plot different ROC bends for a specific scope of T2. To get comes about for ROC bends a preparation set made by 380 pictures taken from various scanners and 380 pictures taken from various advanced

cameras, assorted from the pictures of test-set utilized as a part of Section 5 for the test tests, have been given. The preparation set has been tried by choosing for T2 three qualities (0.1,0.15,0.2) and for each of this edges, the parameter  $\alpha$  runs in  $[0.1, 0.9]$  with ventures of 0.1. This decides the ROC bends figure 5.3.

The range under a ROC bend (AUC) evaluates the general capacity of the test to segregate amongst scanner and computerized camera pictures. A really pointless test (no preferred to recognize genuine positive over flipping a coin) has a relative region of 0.5. An impeccable test (one that has zero false positive and zero false negative) has a relative territory of 1. Genuine tests will exhibit after that a range between these two qualities. As it can be seen, the more prominent AUC is gotten with T2 equivalent to 0.2

Next stride is to break down the single ROC Curve (Figure 5.3). A point in ROC space rules another in the event that it has a higher genuine positive rate and a lower false positive rate. So the best an incentive for  $\alpha$  is the nearest indicate (0,1); for this situation, it is accomplished for  $\alpha$  equivalent to 0.4. At last on the premise of such an examination, in the exploratory tests, the estimations of parameters have been set to the  $\alpha = 0.4$  and T2 = 0.2 individually.

### 3.4 Experimental Tests

Exploratory tests have been done to bolster the hypothetical framework. Computerized pictures originating from 4 different scanners (Epson Expression XL 10000 2400x4200 dpi, HP Scanjet 8300 4800x4800 dpi, HP Deskjet F4180 1200x2400 dpi, Brother DCP 7010 600x2.400 dpi) and from 7 commercial cameras (Canon DIGITAL IXUS i ZOOM, Nikon COOLPIX L12, Fuji Finepix F10, HP Photosmart C935, Nikon D80, Samsung VP-MS11, Sony DSC-P200) have been gained in TIFF and JPEG design. As a result of the assorted size of the

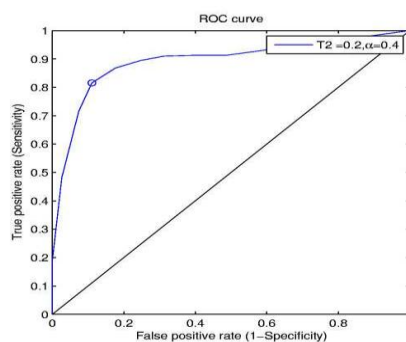
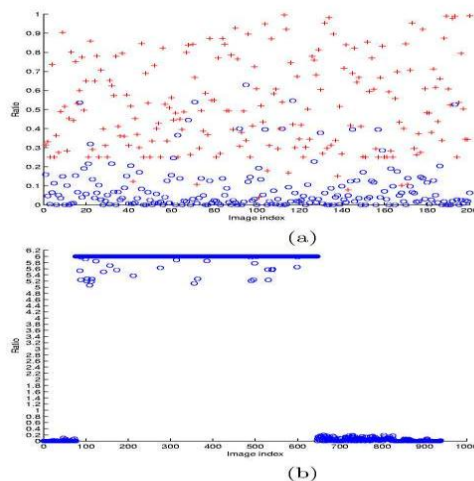


Figure 5.5 The selected ROC Curve

contents, the analysis has been done by dividing them into images of fixed dimension  $N \times M$  ( $1024 \times 768$ ). Obtained results have confirmed theoretical assumptions as it can be seen in figure 5.5 (a) where *RATIO* values are plotted and a separate clustering is observed (for sake of clarity when *RATIO* was over 1 the inverse was taken, due to this, information about scanning direction is lost). In figure 5.5 (b), just examined pictures, accurately identified, are (figure 5.6) for this situation reversal of *RATIO* has not been done and, to make representation less demanding, high values are soaked at 6. It is basically to recognize the two distinctive examining bearings individuated by high and low estimations of *RATIO*; in demanding it is intriguing to take note of the left and the correct side of the plot identified with segment filtering heading and the focal part identified with line course.



**F (a) Energy RATIO for 200 scanned (circle) and 200 camera (cross) images**  
**(b)Energy RATIO only for 950 scanned images, correctly detected**

#### 4. DETECTING CUT-AND-PASTE FORGERIES

In this subsection comes about concerning realness check against the cut-and-glue altering are exhibited. The cut-and-paste strategy comprises of joining picture parts, which originated from various pictures that may be caught by utilizing distinctive gadgets. For the situation when the altered pictures were made by joining an advanced camera picture with a checked picture, or viceversa, can likewise be utilized to recognize such falsifications. Notwithstanding this it is likewise conceivable to distinguish another kind of phony assault, for example, joining parts of two advanced scanner pictures with various filtering bearing. An illustration is appeared in figure 5.6, where it has been made an altered picture by embedding's a piece of a computerized camera picture originating from a Nikon E4600 inside a unique checked picture (HP Deskjet F4180, 600 dpi) of size 2380 × 3550.

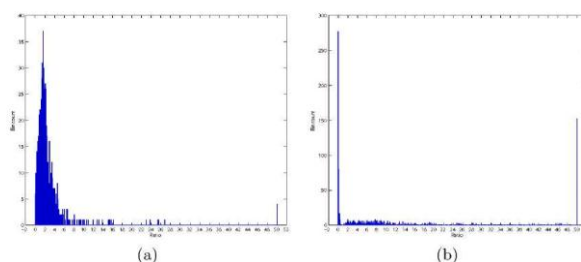


Figure 5.6 Statistical distribution of *RATIO* (a) camera (b) scanned Images

Table 5.7 Confusion matrix for scanned and camera images over a data set of 2000 images (left) and scanning direction recovery for scanner correct answers (right)

	Camera	Scanner		Camera	Scanner
Camera	89.74%	10.26%	Camera	100.00%	0.00%
Scanner	14.65%	85.35%	Scanner	0.00%	100.00%



Figure 5.7 Original scanned (Left) and forged image (Right)

To distinguish the altered district of the photo, the picture is controlled, as per this procedure, by partitioning it into examination pieces of size  $384 \times 512$ , beginning from the upper left corner. 36 sub-pictures are obtained which practically covers the entire picture (a moment check should be possible by beginning from the base right corner) and the figure RATIO each square is ascertained.

Since the first picture has been checked along segment bearing, it is normal that the Energy RATIO of each piece will be little (right around zero). Though a RATIO with qualities more than 0.2, showing that a few sections originated from a camera, are predicted in the altered area.

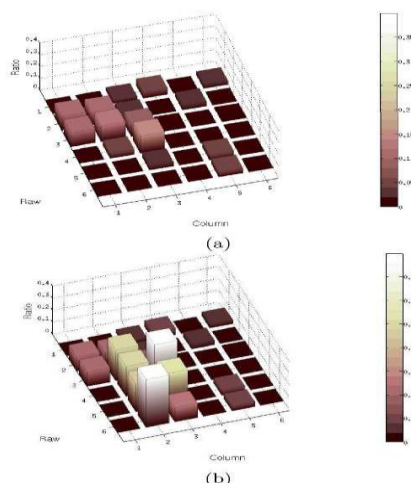


Figure 5.8 The RATIO values of the Figure 5.6 (a) the original image (b) the tampered one

In figure 5.8 (an) and (b), the RATIO estimations of each piece for the first picture and for the altered one are demonstrated individually: each bar of the 3D chart corresponds at one of the 36 squares forming the picture. Hinders with higher qualities than the choice limit T2 set to 0.2 are prove as altered pieces in the changed range. A lot of examinations were performed, making diverse altering pictures with various sizes of the produced territories: the technique can recognize a manufactured fix that includes the 7% (all things considered) of the first picture.

## 5. CONCLUSIONS

We have presented a new method for clustering images based on the PCE similarity scores of their PRNU patterns. It uses interchangeably low-dimensional embedding, interactive visualization and classical clustering. We evaluated the proposed method on the Dresden image database, and the results (presented in Table 2) show its effectiveness. The method does not require parameter tuning in the embedding phase. On the other hand, in the clustering phase

parameters like the number of clusters are easily deducible from the visualization. To the best of our knowledge, this is the first method for clustering images for common source camera detection that uses both embedding and (interactive) visualization. Possibilities for future work include rigorous performance analysis of the image noise patterns embedding, other similarity scores computation algorithms, and testing the proposed method on other datasets.

## 6. REFERENCES

- [ 1] Tang, J., Liu, J., Zhang, M., &Mei,
- [ 2] Q.(2016b). Visualizing large-scale and
- [ 3] high-dimensional data. In Proc. Conf. on
- [ 4] World Wide Web WWW '16 (pp. 287–297). ACM.
- [ 5] Tang, J., Liu, J., Zhang, M., &Mei, Q.(2016b). Visualizing large-scale and high-dimensional data. In Proc. Conf. on World Wide Web WWW '16 (pp. 287–297). ACM.
- [ 6] Anscombe's quartet. [https://en.wikipedia.org/wiki/Anscombe's\\_quartet](https://en.wikipedia.org/wiki/Anscombe's_quartet). Accessed: 13 May 2017.
- [ 7] Aggarwal, C. C., Hinneburg, A., & Keim, D. A. (2001). On the surprising behavior of distance metrics in high dimensional space. In Database Theory—ICDT2001:8thInternationalConferenceLondon,UK,January4–6, 2001 Proceedings (pp. 420–434). Berlin, Heidelberg: Springer Berlin Heidelberg.
- [ 8] Bloy, G. J. (2008). Blind camera fingerprinting and image clustering. *IEEE Transactions on Pattern Analysis and Machine Intelligence*, 30, 532–534.
- [ 9] D. Valsesia, G. Coluccia, T. Bianchi, and E. Magli, “Large-scale image retrieval based on compressed camera identification,” *IEEE Trans. on Multimedia*, vol. 17, no. 9, pp. 1439–1449, 2015.
- [ 10] J. Lukas, J. Fridrich, and M. Goljan, “Determining digital image origin using sensor imperfections,” in Proc. of SPIE - The International Society for Optical Engineering, vol. 5685, 2005, pp. 5685–5685–12.
- [ 11] J. Besag, “On the statistical analysis of dirty pictures,” *The Royal Statistical Society B*, vol. 48, no. 3, pp. 48–259, 1986.
- [ 12] W. Cheney and A. A. Goldstein, “Proximity maps for convex sets,” *The American Mathematical Society*, vol. 10, no. 3, pp. 448–450, 1959.
- [ 13] J. Lukas, J. Fridrich, and M. Goljan, “Digital camera identification from sensor pattern noise,” *IEEE Trans. on Information Forensics and Security*, vol. 1, no. 2, pp. 205–214, 2006.
- [ 14] Q.-T. Phan, G. Boato, F. G.B. De Natale, “Image clustering by source camera via sparse representation,” in Proc. of the 2nd MFSec, 2017, pp. 1–5.
- [ 15] Y.-X. Wang and H. Xu, “Noisy sparse subspace clustering,” *Journal of Machine Learning Research*, vol. 17, no. 12, pp. 1–41, 2016.

- [ 16] R. Li, C.-T. Li, and Y. Guan, “Inference of a compact representation of sensor fingerprint for source camera identification,” *Pattern Recognition*, vol. 74, pp. 556–567, 2018.
- [ 17] D. Valsesia, G. Coluccia, T. Bianchi, and E. Magli, “Compressed fingerprint matching and camera identification via random projections,” *IEEE Trans. on Information Forensics and Security*, vol. 10, no. 7, pp. 1472–1485, 2015.
- [ 18] M. Chen, J. Fridrich, and M. Goljan, “Digital imaging sensor identification (further study),” in *Proc. of SPIE Electronic Imaging, Security, Steganography, Watermarking of Multimedia Contents IX*, vol. 6505, 2007.
- [ 19] Gisolf, F., Barends, P., Snel, E., Malgoezar, A., Vos, M., Mieremet, A., & Geradts, Z. (2014). Common source identification of images in large databases. *Forensic science international*, 244, 222–230.
- [ 20] vanderMaaten,L.(2014). Acceleratingt-SNEusingTree-BasedAlgorithms. *JournalofMachineLearningResearch*, 15,URL:<http://jmlr.org/papers/v15/vandermaaten14a.html>.